

Non local transport through a disordered superconductor: coupling to the condensate

S. Duhot and R. Mélin

Centre de Recherches sur les Très Basses Températures, CRTBT,
CNRS, BP 166, 38042 Grenoble Cedex 9, France*

Considering non local transport through a superconductor from the point of view of the condensate, we find that a spin-up electron from a normal metal entering a superconductor propagates as a composite object consisting of a spin-down hole and a pair in the condensate. This leads to a factorization of the non local conductance as two local Andreev reflections at both interfaces and one propagation in the superconductor, which is tested numerically within a one dimensional toy model of reflectionless tunneling. Because of its pair current component, the non local current is limited by the superconductor critical current. Further evidence of the coupling to the condensate is provided by non local conductance fluctuations, characterized numerically by damped periodic oscillations in the energy dependence of the autocorrelation of the transmission coefficient. The Thouless energies have a weaker dependence on the elastic mean free path than in the normal state, and are inverse proportional to the system size. Weak localization in the superconductor induces a relevant scattering in the Cooper channel that leads to collective modes and a symmetry breaking between the normal and anomalous channels. All the processes considered here receive a simple interpretation in terms of Andreev reflections, either at the interfaces or “internal” to the superconductor.

PACS numbers: 74.50.+r,74.78.Na,74.78.Fk

I. INTRODUCTION

Correlated pairs of electrons can be manipulated in solid state devices by extracting Andreev pairs from a conventional superconductor, being a condensate of Cooper pairs. This process is known as Andreev reflection¹ at a normal metal / superconductor (NS) interface. One considers the future realization of devices designed for manipulating separately one of the two electrons of an Andreev pair and see the feedback on the other electron^{2,3,4,5,6,7}. The question arises of exploring experimentally and understanding theoretically the properties of the simplest of these devices: a source of spatially separated Andreev pairs propagating in different electrodes forming, in short, “non local” Andreev pairs. The possibility of realizing a source of non local Andreev pairs has indeed aroused a considerable interest recently, both theoretical^{2,3,4,5,6,7,8,9,10,11,12,13,14,15,16,17,18} and experimental^{19,20}.

In a theoretical prediction prior to the experiments^{19,20}, Falci *et al.*¹² have obtained from lowest order perturbation theory in the tunnel amplitudes a vanishingly small non local signal with normal metals. Russo *et al.*²⁰ have obtained on the contrary a sizeable experimental non local signal in a three terminal structure consisting of a normal metal / insulator / superconductor / insulator / normal metal (NISIN) tri-layer. The goal of our article is to provide a theory that, together with Ref. 21, can explain this experiment²⁰, and be consistent with the other available experiment by Beckmann *et al.* with ferromagnets¹⁹.

Falci *et al.*¹² have discussed the two competing channels contributing to non local transport. An incoming electron in electrode “b” can be transmitted as an electron in electrode “a”, corresponding to normal transmis-

sion in the electron-electron channel (see the device on Fig. 1 for the labels “a” and “b”). Conversely, it can be transmitted as a hole in electrode “a” while a Cooper pair is transferred in the superconductor. The later transmission in the electron-hole channel corresponds to a dominant “non local” Andreev reflection channel that can lead to spatially separated, spin entangled pairs of electrons. The outgoing particles in the two transmission channels have an opposite charge, resulting in a different sign in the contribution to the current in electrode “a”. With normal metals, not only have the elastic cotunneling and crossed Andreev reflection an opposite sign in the non local conductance, but they are exactly opposite within lowest order perturbation theory in the tunnel amplitudes.

It was already established that non local transport is dominated by elastic cotunneling for localized interfaces¹⁶. The superconductor can essentially be replaced by an insulator for a very thin superconductor connected by tunnel contacts to a normal metal (assuming that the superconductor can still be described by BCS theory). We show that this picture breaks down if the superconductor thickness is larger than the coherence length because transport is mediated by composite objects made of evanescent quasiparticles and pairs in the condensate. The pair current is limited by the critical current, which leads to a disappearance of the non local differential signal above a cross-over voltage V_b^* that is evaluated below in connection with the experiment in Ref. 20.

On the other hand, the coupling to the condensate is obvious in small area junctions leading to fluctuations of the non local conductance. A collective mode^{22,23} is involved in this case. The simulations are explained by the relevant scattering in the Cooper channel induced by

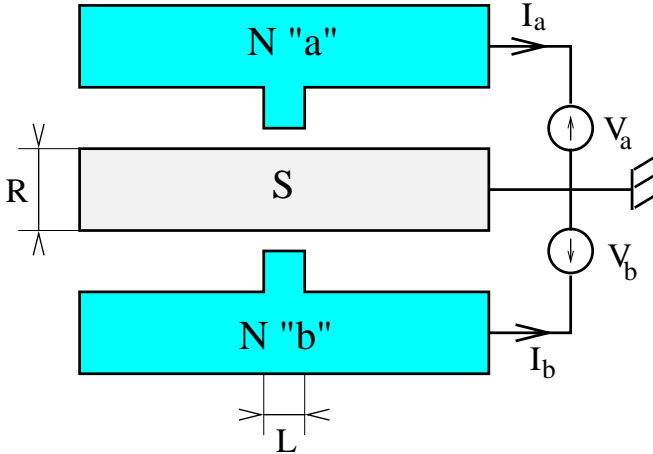


FIG. 1: (Color online.) Schematic representation of the electrical circuit corresponding to the NISIN double interface interpolating between a localized contact for $L \sim \lambda_F$ (with λ_F the Fermi wave-length) and an extended interface for $L \gg L_{\text{th}}(\omega)$, where L_{th} is the Thouless length corresponding to the energy eV_b . The current I_a through electrode “a” is determined in response to a voltage V_b on electrode “b”, with $V_a = 0$. The dimensions R (superconductor thickness) and L (dimension of the junction) are shown on the figure. The available experiment by Russo *et al.* corresponds to extended interface with L of the order of $0.5\mu\text{m}$ and $R \simeq 15 \div 200\text{nm}$.

weak localization in the superconductor.

The article is organized as follows. The factorization of non local processes as two local Andreev reflections and a non local propagation is discussed in Sec. II. The factorization of the non local conductance is illustrated in Sec. III in the case of one dimensional models (the Blonder, Thinkham, Klapwijk (BTK) model and a Green’s function model). The supercurrent is also calculated for the BTK model, which confirms that part of the non local current flows through the condensate. The issue of non local conductance fluctuations is examined in Sec. IV on the basis of numerical simulations showing evidence of collective modes. The connection between non local transport and collective modes is discussed in Sec. V. Concluding remarks are given in Sec. VI.

II. FACTORIZATION OF THE NON LOCAL RESISTANCE

A. Existing results for $eV_b \gg E_{\text{th}}(L)$

The diagram corresponding to the non vanishing lowest order process of order T^4 is shown on Fig. 2a, with T the normal transparency. This diagram is local with respect to excursions parallel to the interfaces if the bias voltage energy eV_b is much larger than the Thouless energy $E_{\text{th}}(L)$ associated to the dimension L of the junction parallel to the interface (see Fig. 1), as it is the case in

the experiment by Russo *et al.*²⁰. The corresponding non local conductance

$$\overline{\mathcal{G}}_{a,b}(V_b) = \frac{\partial I_a}{\partial V_b}(V_b), \quad (1)$$

where I_a and V_b are defined on Fig. 1, is given by^{16,21}

$$\overline{\mathcal{G}}_{a,b}(V_b) = -\frac{e^2}{h} N_{\text{ch}} T^4 \frac{\xi}{l_e^{(S)}} \frac{\Delta^2}{\Delta^2 - (eV_b)^2} \exp \left[-\left(\frac{2R}{\xi} \right) \right], \quad (2)$$

where N_{ch} is the number of conduction channels, Δ is the superconducting gap, $l_e^{(S)}$ the superconductor elastic mean free path, T the normal local transparency, and the overline is an average over disorder. The local Andreev conductance is given by

$$\mathcal{G}_{\text{loc}}(V_b) = 2 \frac{e^2}{h} N_{\text{ch}} T^2 \frac{\Delta^2}{\Delta^2 - (eV_b)^2}, \quad (3)$$

where we used the ballistic result without disorder because of the condition $eV_b \gg E_{\text{th}}(L)$.

The resistance matrix probed in the experiment²⁰ is the inverse of the conductance matrix calculated theoretically:

$$\begin{bmatrix} \mathcal{R}_{a,a}(V_b) & \mathcal{R}_{a,b}(V_b) \\ \mathcal{R}_{b,a}(V_b) & \mathcal{R}_{b,b}(V_b) \end{bmatrix} = \begin{bmatrix} \overline{\mathcal{G}}_{a,a}(V_b) & \overline{\mathcal{G}}_{a,b}(V_b) \\ \overline{\mathcal{G}}_{b,a}(V_b) & \overline{\mathcal{G}}_{b,b}(V_b) \end{bmatrix}^{-1}, \quad (4)$$

from what we deduce that the non local resistance $\mathcal{R}_{a,b}(V_b)$ is given by

$$\mathcal{R}_{a,b}(V_b) = \frac{-\overline{\mathcal{G}}_{a,b}(V_b)}{[\mathcal{G}_{\text{loc}}(V_b)]^2 - \overline{\mathcal{G}}_{a,b}(V_b) \overline{\mathcal{G}}_{b,a}(V_b)}, \quad (5)$$

that simplifies into

$$\mathcal{R}_{a,b}(V_b) \simeq -\frac{\overline{\mathcal{G}}_{a,b}(V_b)}{[\mathcal{G}_{\text{loc}}(V_b)]^2} \quad (6)$$

if the thickness of the superconductor is larger than the superconducting coherence length ξ , and leads to

$$\begin{aligned} \mathcal{R}_{a,b}(V_b) &= \frac{1}{4N_{\text{ch}}} \frac{h}{e^2} \left(\frac{\xi}{l_e^{(S)}} \right) \\ &\times \left(\frac{\Delta^2 - (eV_b)^2}{\Delta^2} \right) \exp(-2d/\xi). \end{aligned} \quad (7)$$

The non local resistance at low bias is positive (dominated by elastic cotunneling), as found in Ref. 16. We do not address here extended interfaces as in Ref. 21 because the pair current considered below is a property of localized interfaces.

B. Case $eV_b \lesssim E_{\text{th}}(L)$

Now, if the bias voltage energy eV_b is smaller than the Thouless energy $E_{\text{th}}(L)$, the lowest order diagram of

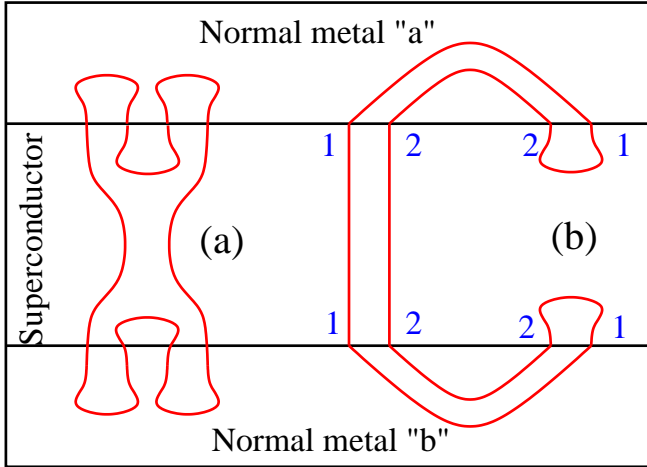


FIG. 2: (Color online.) The diagrams representing the lowest order processes of order T^4 . The diagram (a), local with respect to a propagation in the normal electrodes, was introduced in Ref. 16. The diagram (b) is its non local counterpart. “1” and “2” correspond to the electron and hole Nambu labels. The diagram on (b) factorizes in two Andreev reflections at both interfaces, and a non local propagation in the superconductor. The electron line crosses 8 times the interfaces, so that the diagrams are of order T^4 , where $T \propto (t/\epsilon_F)^2$ is the normal transparency, with t the tunnel amplitude and ϵ_F the Fermi energy.

order T^4 becomes non local in the normal electrodes (see Fig. 2b). The diagram on Fig. 2b corresponds to two Andreev reflections in the normal electrodes, connected by a propagation in the superconductor, so that the non local conductance factorizes into

$$\bar{\mathcal{G}}_{a,b}(V_b) = \frac{\mathcal{S}(V_b) [\mathcal{G}_{\text{loc}}(V_b)]^2}{N_{\text{ch}}}, \quad (8)$$

where $\mathcal{S}(V_b)$ is a transmission coefficient of the superconductor. Using Eq. (6), we find that the crossed resistance

$$\mathcal{R}_{a,b}(V_b) = -\frac{\mathcal{S}(V_b)}{N_{\text{ch}}} \quad (9)$$

does not depend on the local conductances. The scaling between the local and non local conductances is tested in Sec. III for the generalization of the model of reflectionless tunneling at a single interface introduced by Melsen and Beenakker²⁷.

The factorization of the Andreev reflections at both interfaces suggests that part of the current is carried by pairs in the condensate. We thus arrive at the notion of the transport of a composite objects made of an evanescent quasiparticle and a pair in the condensate: an electron from a normal electrode is transmitted in the superconductor as a quasi-hole and a pair in the condensate (see Fig. 3a). The consequences of this qualitative picture are considered below under several complementary points of view.

Finally, we note that the factorization of two Andreev reflections at the interfaces is also valid if $eV_b \gg E_{\text{th}}(L)$ (see Sec. II A), as in the experiment by Russo *et al.*²⁰. This is because the normal Green’s functions are vanishingly small at zero energy in a superconductor.

III. ONE DIMENSIONAL MODELS

A. Blonder, Tinkham, Klapwijk (BTK) approach

1. Non local conductance

Let us now consider a one dimensional model of NISIN double interface within the BTK approach²⁸ (see Fig. 4a). The goal is two-fold: i) obtain the expression of the pair current in the superconductor, and ii) test the factorization of the non local conductance in the case of the model of reflectionless tunneling introduced by Melsen and Beenakker²⁷.

The gap of the superconductor is supposed to have a step-function variation as a function of the coordinate z along the chain: $\Delta(z) = \Delta\theta(z + R/2)\theta(R/2 - z)$, and we suppose δ -function scattering potentials at the interfaces: $V(z) = H\delta(z + R/2) + H\delta(z - R/2)$ ²⁴. The interface transparencies are characterized by the parameter $Z = 2mH/\hbar^2k_F$, where $v_F = \hbar k_F/m$ is the Fermi velocity, with m the electron mass and k_F the Fermi wavevector. The one dimensional model is a simplified version of the genuine three terminal geometry with a supercurrent flow. The current in the normal electrode “a” is not equal to the injected current in electrode “b” because part of the injected current has been converted in a supercurrent.

The unknown coefficients in the expression of the wavefunction are determined from the matching conditions at the interfaces²⁴. Of particular interest are the amplitudes $a'(k_F R)$ and $b'(k_F R)$ of transmission in the electron-hole and electron-electron channels from one normal metal to the other, corresponding respectively to elastic cotunneling and non local Andreev reflection. Assuming $R \gg \xi$, we expand a' and b' to lowest order in $\exp(-R/\xi)$, to find the transmission coefficients

$$\int_0^{2\pi} \frac{d(k_F R)}{2\pi} |a'(k_F R)|^2 = \quad (10)$$

$$\left(\frac{1}{2Z^4} - \frac{1}{2Z^6} + \frac{1}{2Z^8} + \dots \right) e^{-2R/\xi} + \mathcal{O}(e^{-4R/\xi})$$

$$\int_0^{2\pi} \frac{d(k_F R)}{2\pi} |b'(k_F R)|^2 = \quad (11)$$

$$\left(\frac{1}{2Z^4} - \frac{1}{2Z^6} + \frac{5}{4Z^8} + \dots \right) e^{-2R/\xi} + \mathcal{O}(e^{-4R/\xi})$$

at $\omega = 0$. We deduce the first non vanishing term in the large- R , large- Z expansion of the non local transmission:

$$T' = \int_0^{2\pi} \frac{d(k_F R)}{2\pi} (|a'(k_F R)|^2 - |b'(k_F R)|^2) \quad (12)$$

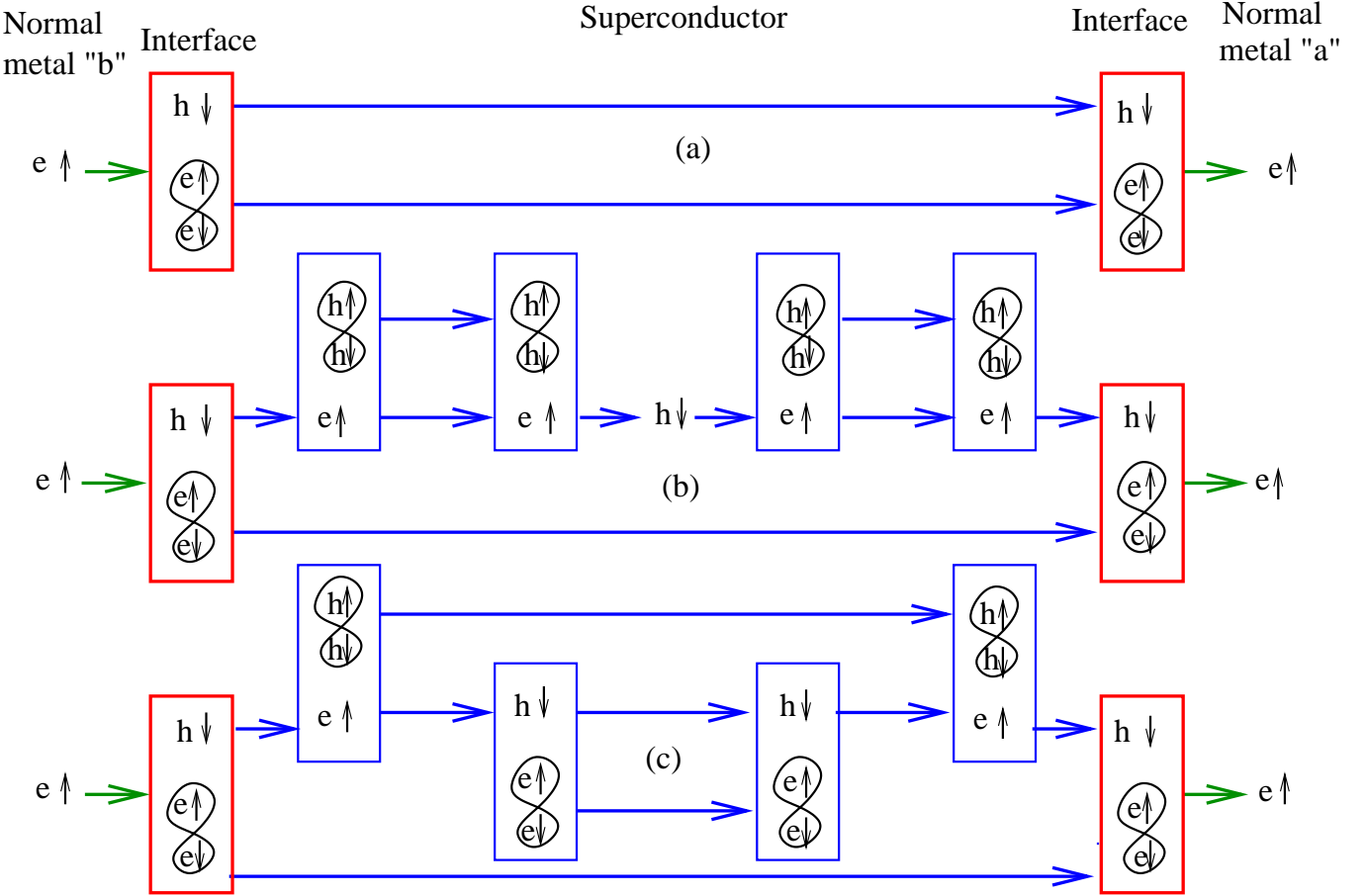


FIG. 3: (Color online.) Schematic representation of (a) the formation of composite objects at the interfaces with a ballistic superconductor; (b) the sequential conversion of the composite objects in the bulk of the superconductor in the absence of weak localization; (c) the scattering in the Cooper channel resulting in a collective mode induced by weak localization.

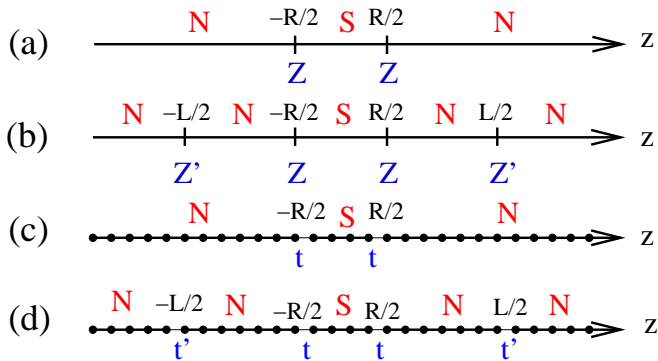


FIG. 4: (Color online.) Schematic representations of the one dimensional models: (a) the BTK model for NISIN and (b) NINISININ junctions, and (c) the tight-binding model for NISIN and (d) NINISININ junctions.

$$= -\frac{3}{4Z^8}e^{-2R/\xi} + \mathcal{O}(e^{-4R/\xi}).$$

In agreement with the Green's function approach^{16,21}

corresponding to the diagrams on Fig. 2, the non local conductance is dominated by elastic cotunneling and appears at order $Z^{-8} \sim T^4$. In agreement with Ref. 16, we find no non local Andreev reflection for highly transparent interfaces corresponding to $Z = 0$.

2. Supercurrent

In the three terminal configuration that we consider, part of the supercurrent is converted as a quasiparticle current at the other interface, as it can be deduced from the supercurrent source term²⁴ related to the right interface, and leading to the supercurrent

$$J_{a,b}^{(S)} = -\frac{16ev_F}{Z_a^4 Z_b^4} \frac{\Delta^3}{(\Delta^2 - \omega^2)^{3/2}}, \quad (13)$$

where Z_a and Z_b are the Z -parameters of both interfaces.

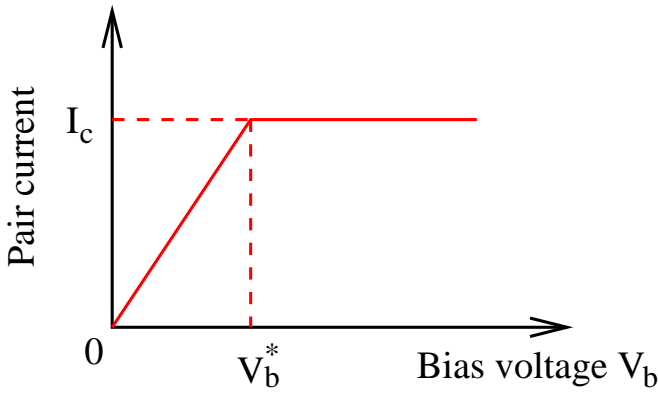


FIG. 5: (Color online.) Schematic representation of the limitation of the pair current (proportional to the non local current) by the critical current I_c of the superconductor. The superconducting gap is supposed to be independent on the bias voltage V_b .

3. Comparison to experiments

The component of the supercurrent carried by pairs cannot exceed the superconductor critical current. Therefore, the non local current saturates at $V_b = V_b^*$ (see Fig. 5) and the differential non local conductance vanishes for $V_b > V_b^*$. Noting $V_b^*(R)$ the dependence of V_b^* on the thickness R of the superconductor, we impose

$$N_{\text{ch}} \frac{e^2}{h} \Delta \propto \int_0^{V_b^*(R)} |\bar{\mathcal{G}}_{a,b}(V_b')| \exp(-2R/\xi) d(eV_b'). \quad (14)$$

The proportionality factor relating the supercurrent to the non local current is not relevant to the forthcoming Eq. (15). For the sake of a qualitative discussion, we suppose $\bar{\mathcal{G}}_{a,b}(V_b') = \bar{\mathcal{G}}_{a,b}$ for $V_b' < V_b^*(R)$, and $\bar{\mathcal{G}}_{a,b}(V_b') = 0$ for $V_b' > V_b^*(R)$. Eq. (6) leads to

$$\frac{V_b^*(R_1)}{V_b^*(R_2)} = \frac{\mathcal{R}_{a,b}(R_2) \exp(2R_2/\xi)}{\mathcal{R}_{a,b}(R_1) \exp(2R_1/\xi)}. \quad (15)$$

Compared to the experiments²⁰, for $R_1 = 15 \text{ nm}$, $R_2 = 50 \text{ nm}$, $\mathcal{R}_{a,b}(R_1) = 0.3 \Omega$, $\mathcal{R}_{a,b}(R_2) = 25 \text{ m}\Omega$, we find $V_b(R_1)/V_b(R_2) \simeq 8$ while a value of order 5 is obtained in the experiment with $V_b^*(R_1) \simeq 0.5 \text{ mV}$, $V_b^*(R_2) \simeq 0.1 \text{ mV}$ and $\xi = 15 \text{ nm}$. The absolute value of the crossed resistance at zero bias is also in agreement with Eq. (2) from our model (a detailed discussion is presented in Ref. 21). Our interpretation, in a quantitative agreement with experiments, is not related to the normal state Thouless energy even though, numerically, eV_b^* appears to be close to the normal state Thouless energy for the two thickness considered in the experiment²⁰. This predicted absence of a relation between eV_b^* and the normal state Thouless energy may be tested experimentally by varying the number of channels N_{ch} , proportional to the area of the junction.

B. Reflectionless tunneling

1. BTK approach

To discuss the form (9) of the crossed resistance, we include now multiple scattering in the normal electrodes and consider two additional scatterers at positions $z_1 = -L_1/2$ in the left electrode and $z_2 = L_2/2$ in the right electrode, described by the potentials $V'(z) = H'\delta(z - z_1) + H'\delta(z - z_2)$, and leading to the barrier parameter $Z' = 2mH'/\hbar^2k_F$ (see Fig. 4b for the definitions of Z and Z'). This constitutes, for a double interface, the analog of the model introduced by Melsen and Beenakker²⁷ for a single interface. We average numerically the non local transmission coefficient over the Fermi oscillation phases $\varphi_1 = k_F(R - L_1)/2$, $\varphi = k_F R$ and $\varphi_2 = k_F(L_2 - R)$.

The variations of the non local conductance at zero bias as a function of Z' for a fixed Z are shown on Fig. 6, as well as the corresponding non local conductance for the NINISIN junction. The negative non local conductance at small Z_1 for the NINISIN junction disappears when increasing the precision of the integrals. The variation of the non local conductance on Fig. 6 shows a strong enhancement by the additional scatterers, like reflectionless tunneling at a single NIS interface²⁷.

2. Green's functions: scaling between the local and non local conductances

Considering the tight-binding model within Green's functions, the variation of the non local conductance of the NINISIN junction as a function of t' for a fixed t (see Fig. 4d) is similar to the BTK model. Imposing the same normal conductance in the BTK and in the tight-binding models leads to $Z = (1 - (t/T)^2)/(2t/T)$, where T is the bulk hopping amplitude. The identification of Z to t/T results in a good (but not perfect) agreement for the non local conductance when the tight-binding and BTK results are rescaled on each other. The non local conductance $\mathcal{G}_{a,b}(V_b = 0, t/T, t'/T)$ is shown on Fig. 8 as a function of the local conductance $\mathcal{G}_{\text{loc}}(V_b = 0, t/T, t'/T)$, fitted by $\mathcal{G}_{a,b}(V_b = 0, t/T, t'/T) = \mathcal{S}(V_b = 0) [\mathcal{G}_{\text{loc}}(V_b = 0, t/T, t'/T)]^2$, corresponding to Eq. (9) for $N_{\text{ch}} = 1$. The scaling is very well obeyed, showing the validity of form (9) of the crossed resistance involving the destruction of a pair in the condensate at one interface, its propagation in the superconductor and its creation at the other interface.

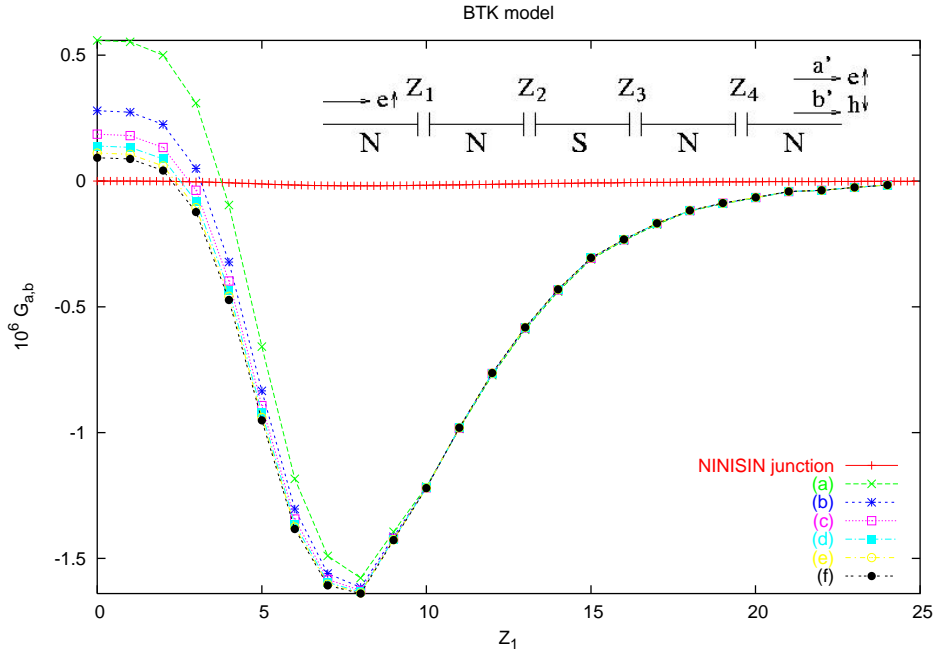


FIG. 6: (Color online.) Variation of the non local conductance $G_{a,b}$ (in units of e^2/h) for the junction on Fig. 4c, with $Z' = Z_1 = Z_4$ and $Z = Z_2 = Z_3 = 10$. (a) ... (f) correspond to an increasing values of the precision in the evaluation of the Fermi phase factors related to the superconductor. We have also shown the much smaller non local conductance of the NINISIN junction, as a function of Z_1 for the NIN contact, with the same value of Z for the NIS contacts.

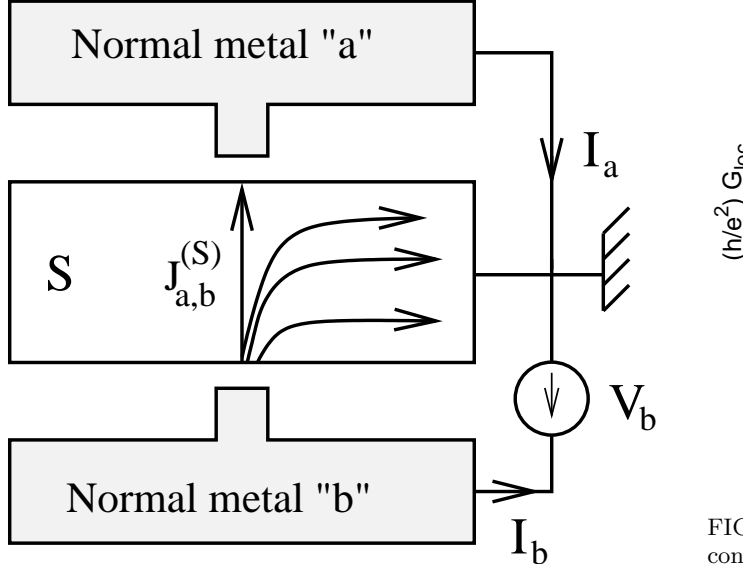


FIG. 7: (Color online.) Schematic representation of the supercurrent flow in two dimensions. We evaluate from the one dimensional BTK model the part $J_{a,b}^{(S)}$ of the supercurrent that flows from electrode "b" to "a".

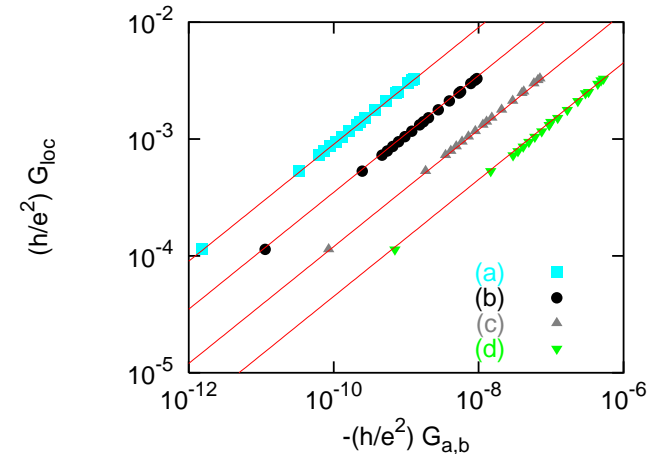


FIG. 8: (Color online.) Correlation between the nonlocal conductance (x -axis) and the local conductance (y -axis) for the peaks similar to Fig. 6 as a function of t'/T for a fixed $t/T = 0.05$ and (a) $R/\xi = 5$, (b) $R/\xi = 4$, (c) $R/\xi = 3$, and (d) $R/\xi = 2$. The solid line is a fit to $G_{a,b}(t'/T) \propto [G_{loc}(t'/T)]^2$.

IV. NON LOCAL CONDUCTANCE FLUCTUATIONS: NUMERICAL RESULTS

A. Introduction

1. Relevance to experiments

We consider now non local conductance fluctuations, that provide additional evidence of the coupling of non local transport to the condensate. The root mean square of the non local conductance fluctuations is proportional to $(e^2/h)T^2$ while the average non local conductance is proportional to $(e^2/h)T^4N_{\text{ch}}$ (see Eq. 2). The fluctuations are important for small junctions such that $T^2N_{\text{ch}} \lesssim 1$.

2. The different length scales in the simulations

The non local transport simulations are carried out in a quasi-1D geometry, on a strip of longitudinal dimension L and of transverse dimension L_y , corresponding to M transverse modes. We calculate non local transport along the z direction. The trilayer geometry with an aspect ratio similar to the experiment by Russo *et al.*²⁰, would require much larger system sizes to have a reasonable separation between the different length scales in the y direction while L is much larger than L_y . The relevant length scales in the diffusive regime are given by increasing order by the Fermi wave-length λ_F , the elastic mean free path l_e , the superconducting coherence length ξ and the sample size.

3. Thouless energy

The Thouless energy is defined from the non local conductance fluctuations by the decay of the autocorrelation of the non local conductance

$$\langle \left[\overline{\mathcal{G}_{a,b}(\omega)\mathcal{G}_{a,b}(\omega + \delta\omega)} - \overline{\mathcal{G}_{a,b}(\omega)}\overline{\mathcal{G}_{a,b}(\omega + \delta\omega)} \right] \rangle_{\omega} \quad (16)$$

as $\delta\omega$ increases, where $\langle \dots \rangle_{\omega}$ denotes an average over the energy ω in a given window.

B. Ballistic system and small disorder

We use typically $M = 10$, L/a_0 ranging from 80 to 100 with a method based on the inversion of the Dyson matrix, and much higher values of L/a_0 (in units of the tight binding model lattice spacing a_0), with a method consisting in connecting together several conductors by a hopping self-energy, given that the Green's functions of each conductor is evaluated by the inversion of the Dyson matrix. This method allows also to evaluate spatial and energy fluctuations of the pair current in the condensate. We also tried recursive Green's function.

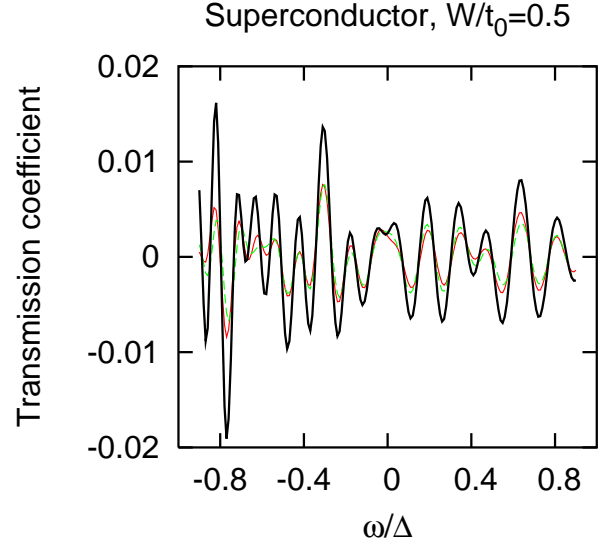


FIG. 9: (Color online.) Energy dependence of the superconducting transmission coefficient $T'(\omega/\Delta)$ [defined by Eq. (17)] through a diffusive superconductor on a strip with $L_y/a_0 = 10$ and $L/a_0 = 100$, in the limit of small disorder. The bold line corresponds to the ballistic result, and the two other traces correspond to two realizations of disorder with $W/t_0 = 0.5$ and $l_e/a_0 \simeq 500$. The ballistic coherence length is $\xi/a_0 \simeq 33$. This figure has been obtained with a method based on the inversion of the Dyson matrix.

The decay length of the ballistic Green's functions in the recursive method cannot be fixed to $\hbar v_F/\Delta$, contrary to the inversion method based on Green's functions in real space where the decay length of the one particle Green's function is a parameter independent from $\hbar v_F/\Delta$. In the simulation Δ is not small compared to the bandwidth, so that, unfortunately, the Green's functions in the recursive method are numerically too small to provide reliable results.

The normalized transmission coefficient $T'(\omega)$ that we calculate numerically is related to the non local conductance by the relation

$$T'(\omega) = \frac{\hbar}{e^2} T^{-2} \mathcal{G}_{a,b}^{(2)}(\omega), \quad (17)$$

where $\mathcal{G}_{a,b}^{(2)}(\omega)$ is the contribution of order T^2 to the non local conductance, with T the normal transparency. The transmission coefficient $T'(\omega)$ defined by Eq. (17) fluctuates around zero as a function of energy because the wave-vectors of the different channels vary with energy. The characteristic energy scale in the oscillations of the transmission coefficient is the ballistic normal state Thouless energy associated to the dimension L (see Fig. 9 in the forthcoming section IV C 1).

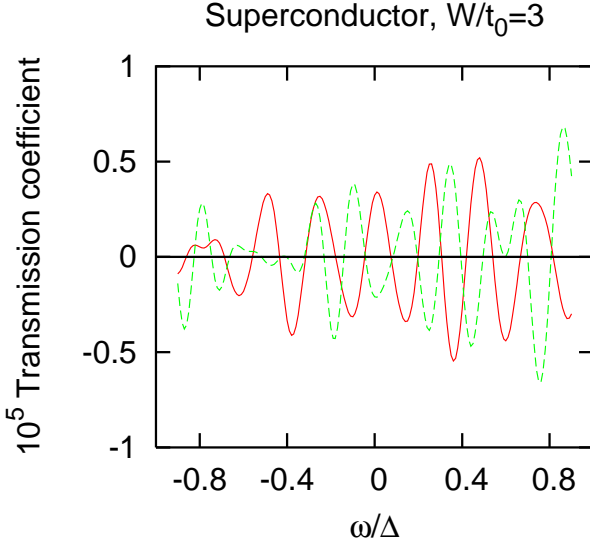


FIG. 10: (Color online.) Energy dependence of the superconducting transmission coefficient $T'(\omega/\Delta)$ [defined by Eq. (17)] through a diffusive superconductor on a strip with $L_y/a_0 = 10$ and $L/a_0 = 100$, in the diffusive limit. The two traces correspond to different realizations of disorder corresponding to $W/t_0 = 3$ and $l_e/a_0 \simeq 16$. This figure has been obtained with a method based on the inversion of the Dyson matrix.

C. Diffusive system

1. Thouless energies in the superconducting case

Figs. 9 and 10 show the energy dependence of the superconducting transmission coefficient $T'(\omega/\Delta)$ defined by Eq. (17). The fluctuations of the transmission coefficient are close to the ballistic limit result in the limit of small disorder (see Fig. 9). We obtain regular fluctuations of the transmission coefficient of a superconductor in the diffusive limit where the normal transmission coefficient is characterized by fluctuations (see Fig. 10). We used a large number of realizations of disorder at a single energy to show that the transmission coefficient averages to zero because of disorder. This shows that the regular fluctuations in the disordered system are genuinely related to disorder, and do not have the same origin as in the ballistic system.

To characterize the regular fluctuations, we calculate the normalized autocorrelation of the transmission coefficient $\mathcal{C}(\delta\omega) = \langle A(\omega, \delta\omega)/B(\omega, \delta\omega) \rangle_\omega$, with

$$A(\omega, \delta\omega) = \overline{T'(\omega + \delta\omega)T'(\omega)} \quad (18)$$

$$B(\omega, \delta\omega) = \sqrt{\overline{T'(\omega + \delta\omega)T'(\omega)}}, \quad (19)$$

where $\langle \dots \rangle_\omega$ is an average over the energy ω , as in Eq. (16). The autocorrelation $\mathcal{C}(\delta\omega)$ is characterized by oscillatory damped oscillations (see Fig. 11), in contrast to the autocorrelation of conductance fluctuations in the

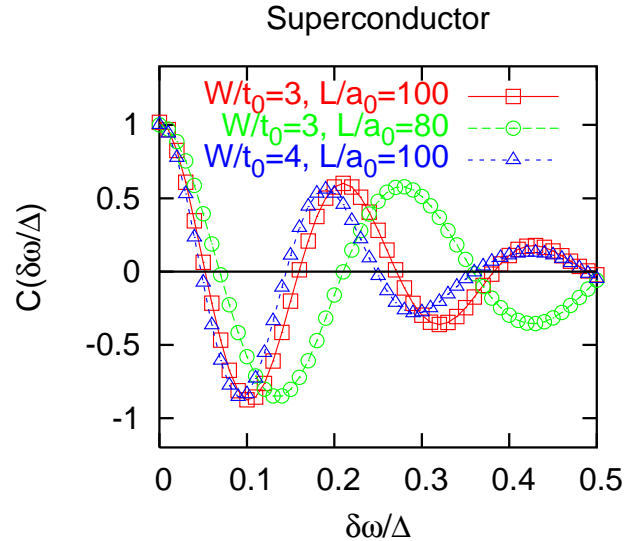


FIG. 11: (Color online.) Autocorrelation function of the transmission coefficient [see Eqs. (18)-(19)], for $(W/t_0 = 3, L/a_0 = 80)$, $(W/t_0 = 3, L/a_0 = 100)$, and $(W/t_0 = 4, L/a_0 = 100)$. $W/t_0 = 3$ corresponds to $l_e/a_0 \simeq 16$, and $W/t_0 = 4$ corresponds to $l_e/a_0 \simeq 10$. The errorbars are smaller than the size of the symbols.

normal case that is damped without oscillations. The energy scales $E_{c,1}$ and $E_{c,2}$ related to period of oscillations and to the damping increase as the system size decreases (see Fig. 11), in agreement with the expected behavior for Thouless-like energies. Going to larger system sizes, we find that $E_{c,1}$ scales like the inverse of the sample size (see Fig. 12).

The comparison between Fig. 10 for $(W/t_0 = 3, l_e/a_0 \simeq 16)$, and similar data for $(W/t_0 = 2, l_e/a_0 \simeq 34)$ and $(W/t_0 = 4, l_e/a_0 \simeq 10)$ show that $E_{c,1}$ and $E_{c,2}$ have a weaker dependence on the elastic mean free path than for a normal diffusive system.

2. Fluctuations of the supercurrent

We consider a superconductor made of $K + 1$ samples of length L_0 connected to each other by highly transparent interfaces, and evaluate the quasiparticle current at energy ω $I_{qp}^{(n)}(\omega)$ through the cross-sections at positions nL_0 (see Fig. 13). As it is visible on Fig. 14, we find i) fluctuations in the energy dependence of the quasiparticle current, and ii) $I_{qp}^{(n)}(\omega) \neq I_{qp}^{(n+1)}(\omega)$, meaning also fluctuations in the supercurrent. This is an additional evidence of the coupling between the evanescent quasiparticle channels and the supercurrent.

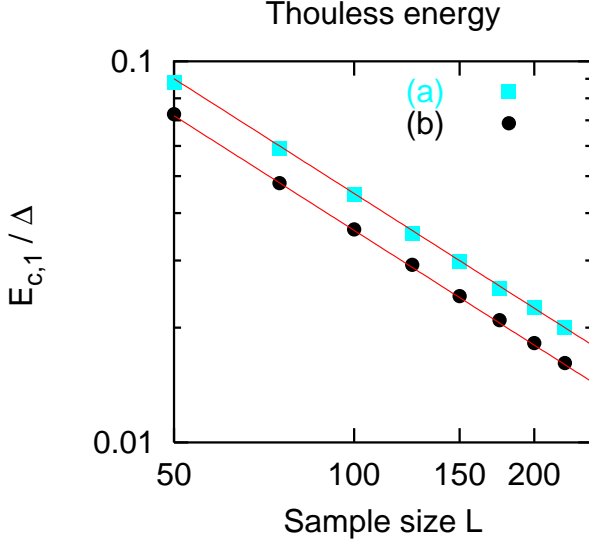


FIG. 12: (Color online.) Variation of the Thouless energy $E_{c,1}/\Delta$ as a function of the system size L/a_0 in a log-log plot, for (a): $W/t = 1$ and $l_e/a_0 \simeq 127$ (b): $W/t = 2$ and $l_e/a_0 \simeq 34$. The solid lines are a fit to $E_{c,a}/\Delta \sim 1/L$.

3. Summary of the numerical results

To summarize, we have shown that

1. The superconducting Thouless energies have a weaker dependence on the elastic mean free path as in the normal case.
2. The superconducting Thouless energies are inverse proportional to the system size, while the normal state Thouless energy is inverse proportional to the square of the system size.
3. The supercurrent fluctuates in space, showing a coupling between the supercurrent and the channel of evanescent quasiparticles.

We provide now the relation between collective modes and these numerical experiments on non local conductance fluctuations.

V. NON LOCAL CONDUCTANCE FLUCTUATIONS: ANALYTICAL RESULTS

A. Diffusons in a superconductor

1. Evaluation of the diffusons

Let us first evaluate the Thouless energy of a superconductor in the absence of crossings between diffusons. Smith and Ambegaokar³¹ start from one extremity of the ladder diagram and calculate recursively the integrals over the wave-vectors. Once the right-most integral

on Fig. 15 has been evaluated, one is left with a “ladder” with one less rung, but with a different 2×2 matrix at the extremity. The four parameter recursion relations reduce to a matrix geometric series in the sector $(\hat{\tau}_0, \hat{\tau}_1)$, and to another matrix geometric series in the sector $(\hat{\tau}_2, \hat{\tau}_3)$, where $\hat{\tau}_n$ are the four Pauli matrices, with $\hat{\tau}_0$ the identity.

More precisely, we define the four matrix diffusons

$$\bar{\mathcal{D}}_{q,\delta\omega}(\hat{\tau}_n) = v^2 \int \frac{d^3\mathbf{k}}{(2\pi)^3} \overline{\hat{\tau}_3 \hat{G}(\mathbf{k}, \omega) \hat{\tau}_n \hat{G}(\mathbf{k} + \mathbf{q}, \omega + \delta\omega) \hat{\tau}_3}, \quad (20)$$

where $n = 0, \dots, 3$, $q = |\mathbf{q}|$ is the modulus of the wave-vector, and $\delta\omega$ is small compared to the energy ω . The microscopic disorder scattering potential is given by $v^2 = 4\pi\epsilon_F/\tau_e$, with ϵ_F the Fermi energy and τ_e the elastic scattering time, related to the elastic scattering length l_e by the relation $l_e = v_F\tau_e$. We find

$$\bar{\mathcal{D}}_{q,\delta\omega}(\hat{\tau}_0) = X (\Delta^2 \hat{\tau}_0 - \omega \Delta \hat{\tau}_1) \quad (21)$$

$$\bar{\mathcal{D}}_{q,\delta\omega}(\hat{\tau}_1) = X (\omega \Delta \hat{\tau}_0 - \omega^2 \hat{\tau}_1), \quad (22)$$

in the sector $(\hat{\tau}_0, \hat{\tau}_1)$, and

$$\begin{aligned} \bar{\mathcal{D}}_{q,\delta\omega}(-i\hat{\tau}_2) &= X \left(-\frac{3\mathcal{D}_0 \Delta \delta\omega \sqrt{\Delta^2 - \omega^2}}{2v_F^2} \hat{\tau}_3 - i(\Delta^2 - \omega^2) \hat{\tau}_2 \right) \\ \bar{\mathcal{D}}_{q,\delta\omega}(\hat{\tau}_3) &= X \mathcal{D}_0 \delta\omega \left(-\frac{\mathcal{D}_0^2 \Delta \delta\omega}{4v_F^4} \hat{\tau}_3 - \frac{3i\Delta}{2v_F^2} \sqrt{\Delta^2 - \omega^2} \hat{\tau}_2 \right), \end{aligned} \quad (23)$$

in the sector $(\hat{\tau}_2, \hat{\tau}_3)$. We used the notation

$$\frac{1}{X} = \frac{3\mathcal{D}_0(\Delta^2 - \omega^2)}{v_F^2} \left[\sqrt{\Delta^2 - \omega^2} + \frac{\mathcal{D}_0 q^2}{4} - \frac{\omega \delta\omega}{2\sqrt{\Delta^2 - \omega^2}} \right], \quad (24)$$

where \mathcal{D}_0 is the diffusion constant.

2. Non local transmission coefficient

The relation between the diffusons in the superconductor and non local transport is provided by the non local conductance (1). The non local conductance $\mathcal{G}_{a,b}^{(2)}(\omega)$ of order T^2 introduced in Eq. (17) is related to the transmission coefficients according to

$$\mathcal{G}_{a,b}^{(2)}(\omega) = \frac{e^2}{h} \left[T_{(1,1)}^{(1,1)}(\omega) - T_{(1,1)}^{(2,2)}(\omega) \right], \quad (25)$$

with

$$\begin{aligned} T_{(\sigma_A, \sigma_R)}^{(\sigma'_A, \sigma'_R)}(\omega) &= T^2 \epsilon_F^2 \int \frac{d^3\mathbf{q}}{(2\pi)^3} e^{i\mathbf{q} \cdot \mathbf{R}} \\ &\times \int \frac{d^3\mathbf{k}}{(2\pi)^3} \overline{\hat{G}^{\sigma_A, \sigma'_A}(\mathbf{k}, \omega) \hat{G}_{\beta, \alpha}^{\sigma'_R, \sigma_R}(\mathbf{k} + \mathbf{q}, \omega)}. \end{aligned} \quad (26)$$

The notation $T_{(\sigma_A, \sigma_R)}^{(\sigma'_A, \sigma'_R)}(\omega)$ corresponds to the transmission coefficient related to a diffuson with the Nambu labels (σ_A, σ_R) for the advanced and retarded propagators

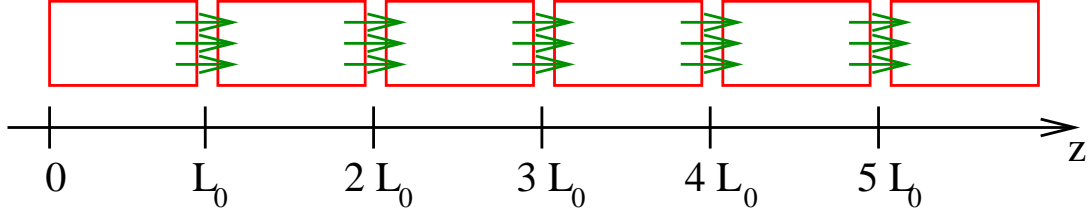


FIG. 13: (Color online.) The geometry in which superconductors of length L_0 are connected to each other by highly transparent interfaces. The quasiparticle current flowing from one conductor to the next is not conserved and fluctuates (see Fig. 14), showing that part of the current is carried by the condensate.

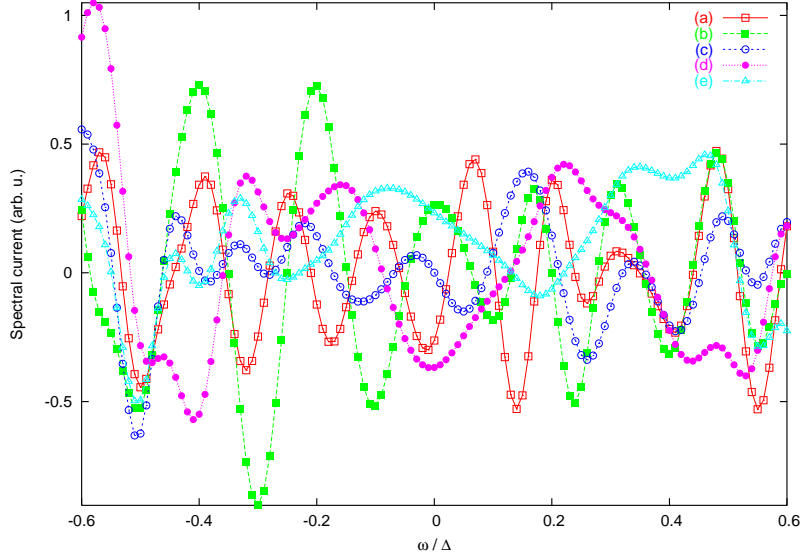


FIG. 14: (Color online.) Quasiparticle spectral current across sections at nL_0 , with $L_0/a_0 = 50$, and (a) $n = 1$, (b) $n = 2$, (c) $n = 3$, (d) $n = 4$, (e) $n = 5$, for a superconductor of total length $6L_0$ (see the geometry on Fig. 13).

at one extremity, and the Nambu labels (σ'_A, σ'_R) at the other extremity (see Fig. 15). The transmission coefficients $\bar{T}_{(1,1)}^{(1,1)}(\omega)$ and $\bar{T}_{(1,1)}^{(2,2)}(\omega)$ encode elastic cotunneling and non local Andreev reflection respectively. We deduce from Eq. (24) that $\bar{G}_{a,b}(\omega) = 0$: the average non local conductance vanishes to order T^2 , in agreement with Sec. II, and with an early work¹³ in the disordered case. The transmission coefficients $\bar{T}_{(1,2)}^{(1,2)}(\omega)$ and $\bar{T}_{(2,1)}^{(2,1)}(\omega)$ involve the propagation of a pair in the condensate in parallel to the quasiparticle channels, as in the diagram on Fig. 2b.

3. Non local conductance fluctuations

The autocorrelation of the non local conductance defined by Eq. (16) is related to the autocorrelation of the transmission coefficients

$$\begin{aligned} &\overline{T_{(\sigma_1, \sigma_2)}^{(\sigma'_1, \sigma'_2)}(\omega) T_{(\sigma_3, \sigma_4)}^{(\sigma'_3, \sigma'_4)}(\omega + \delta\omega)} \\ &-\overline{T_{(\sigma_1, \sigma_2)}^{(\sigma'_1, \sigma'_2)}(\omega) T_{(\sigma_3, \sigma_4)}^{(\sigma'_3, \sigma'_4)}(\omega + \delta\omega)} \rangle_{\omega}. \end{aligned} \quad (27)$$

We deduce from Eqs. (21)-(24) that the Thouless energy is larger than the superconducting gap Δ in the absence of the diffuson crossing (the average of four Green's functions in Eq.(16) is factorized in the product of two averages of two Green's functions). The Thouless energy E_c is indeed determined by the condition

$$\sqrt{\Delta^2 - \omega^2} = \frac{\omega E_c}{2\sqrt{\Delta^2 - \omega^2}}, \quad (28)$$

leading to $E_c = 2\sqrt{\Delta^2 - \omega^2}/\omega$. Therefore, the subgap non local conductance does not fluctuate within this picture. We examine now how this is modified by weak localization.

4. Collective modes

Collective modes^{22,23,32,33,34} correspond to the action of the operator $\rho_{\mathbf{k},\sigma}^{\mathbf{q}} = c_{\mathbf{k}+\mathbf{q},\sigma}^+ c_{\mathbf{k},\sigma}$ (where σ is the spin, k and q are wave-vectors with $|k|$ of order k_F and $|q|$ is much smaller than k_F) on the superconductor ground state^{22,23}. The Anderson-Bogoliubov (AB) mode corre-

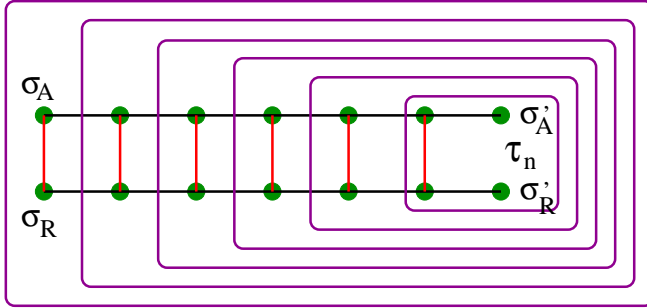


FIG. 15: (Color online.) Schematic representation of the recursive calculation of the matrix diffuson in the ladder approximation used by Smith and Ambegaokar³¹. The integrals over the wave-vectors are carried out recursively, starting from the right of the diagram. The two horizontal black lines correspond to the advanced and retarded Green's functions. The green dots correspond to the disorder vertices, and the vertical red lines correspond to the impurity lines. We have shown the Nambu labels (σ_A, σ_R) and (σ'_A, σ'_R) at the extremities of the diffuson.

sponds to oscillations of the phase of the order parameter, with a dispersion relation

$$\omega_{AB}(q) = \frac{v_F q}{\sqrt{3}} \quad (29)$$

for a ballistic system in the absence of long range Coulomb interactions. On the other hand, non local transport can be seen as the action of $c_{\mathbf{x},\sigma}^+ c_{\mathbf{y},\sigma}$ on the superconductor ground state, where \mathbf{x} and \mathbf{y} are two point on each interface, which suggests the relation between local transport and collective modes that we discuss now.

More precisely, we base our discussion on the Kulik *et al.* article on linear response theory of collective modes³⁴. The starting point Hamiltonian in Ref. 34 is the BCS Hamiltonian \mathcal{H}_0 , perturbed by the Hamiltonian \mathcal{H}' :

$$\mathcal{H}_0 = \sum_{\mathbf{k}} A_{\mathbf{k}}^+ \hat{\epsilon}_{\mathbf{k}} A_{\mathbf{k}} \quad (30)$$

$$\mathcal{H}' = \sum_{\mathbf{k},\mathbf{q}} A_{\mathbf{k}+\mathbf{q}}^+ (\Delta_1 \hat{\tau}_1 + \Delta_2 \hat{\tau}_2 + e\phi \hat{\tau}_3) A_{\mathbf{k}} \exp(-i\omega t) + h.c., \quad (31)$$

where h.c. corresponds to the hermitian conjugate, and where $A_{\mathbf{k}}^+ = [a_{\mathbf{k},\uparrow}, a_{-\mathbf{k},\downarrow}^+]$, and $\hat{\epsilon}_{\mathbf{k}} = \xi_{\mathbf{k}} \hat{\tau}_3 - \Delta \hat{\tau}_1$, with $\xi_{\mathbf{k}}$ the kinetic energy with respect to the Fermi level. We show in section V B that an initial $\Delta_2 \hat{\tau}_2$ perturbation leads to very large weak localization corrections to the diffusion coefficient, and in particular to a very large renormalized $T_{(1,1)}^{(1,1)} - T_{(1,1)}^{(2,2)}$. This shows that the AB mode is relevant because of weak localization, leading to a symmetry breaking between the normal and anomalous channels in non local transport that explains the numerical simulations in Sec. IV.

B. Self-crossing of a diffuson

We evaluate the self-crossing of a diffuson, related to the Gorkov-Larkin-Khmel'nitskii-Hikami (GLKH) box^{35,36,37} on Fig. 16. The average of the product of two advanced Green's functions is limited by the superconducting coherence length ξ in a superconductor²¹, not by the elastic mean free path as in a normal metal. We are thus lead to the diagram on Fig. 16a, containing the insertion of a Cooperon. The value of this diagram in the superconducting case is enhanced by orders of magnitude as compared to the normal case because of the large factor related to the many paths associated to the internal Cooperon.

We evaluate numerically the sum of the GLKH boxes corresponding to Fig. 16b, and to the three others obtained by symmetries, leading to the transmission coefficients $T_{(\sigma_A, \sigma_R)}^{(\sigma'_A, \sigma'_R)}(\omega)$ associated to the diagram on Fig. 16c. We first find that, after the summation over the internal Nambu labels $\{\sigma_i\}$ of the diagram on Fig. 16c, the transmission coefficients $\tilde{T}_{(\sigma_A, \sigma_R)}^{(\sigma'_A, \sigma'_R)}(\omega)$ is much smaller than $T_{(\sigma_A, \sigma_R)}^{(\sigma'_A, \sigma'_R)}(\omega)$. However, we find numerically that each term with a specific value of the internal Nambu labels $\{\sigma_i\}$ is very large. If an asymmetry between the normal and anomalous channels is introduced in the internal diffuson of the diagram on Fig. 16c, we obtain as a result a large asymmetry between the normal and anomalous channels in the total transmission coefficients for the weak localization diagram on Fig. 16c. The perturbation $\Delta_2 \hat{\tau}_2$ encoding the AB mode in Eq. (31) is thus relevant once weak localization is included, explaining the collective mode in the non local conductance simulations in Sec. IV. This mode receives the interpretation of the scattering in the Cooper channel represented schematically on Fig. 3c.

VI. CONCLUSIONS

To conclude, we have provided a theory of non local transport at normal metal / superconductor double interfaces. The central role is played by higher order processes in the tunnel amplitude for which part of the non local current circulates as pairs in the condensate, not only as evanescent quasiparticles. The pair current through a superconductor is limited by the critical current, leading to an upper bias voltage V_b^* above which the non local differential signal disappears, while the total non local current integrated over energy saturates. The pair current appears naturally both in the Green's function and in the BTK descriptions. As a consequence, the crossed conductance at zero bias factorizes in the Andreev conductances at the two interfaces, and a factor related to the propagation in the superconductor. This factorization was tested in the context of a model of reflectionless tunneling²⁷.

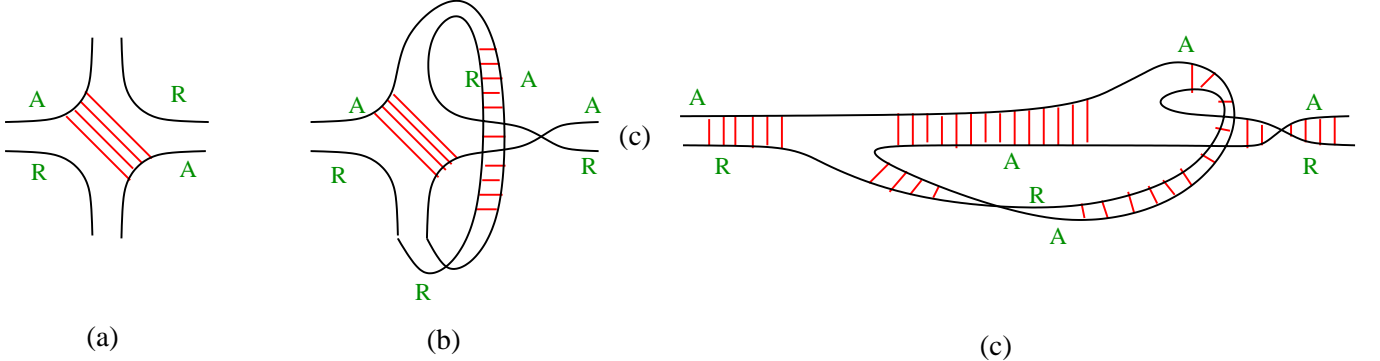


FIG. 16: (Color online.) (a) One of the Gorkov-Larkin-Khmelnitskii-Hikami (GLKH) boxes in the superconducting case, dressed by a diffuson. (b) The self-crossing of a diffuson with the superconducting GLKH box. (c) Another representation of (b), with two additional diffusons at the entry and exit of the GLKH box. “A” and “R” stand for advanced and retarded.

On the other hand, the coupling to the condensate is obvious in the case of non local conductance fluctuations that could be observed in small area junctions. We found regular fluctuations of the non local conductance, that receive an interpretation in terms of collective modes induced by weak localization in the superconductor. Long range Coulomb interactions open a gap in the collective mode spectrum in three dimensions but not in two dimensions. The experimental quasi-two-dimensional geometry will be discussed elsewhere. The effect discussed in Secs. II and III for the average non local resistance in the existing experiment²⁰ is independent on the presence or absence of a gap in the spectrum of collective modes.

Finally, a supercurrent crossing a superconductor in-

duces a phase gradient that can possibly destroy superconductivity above V_b^* . This breakdown of superconductivity would induce a voltage-dependent self-consistent superconducting gap, and a change a sign of the non local resistance from elastic cotunneling to crossed Andreev reflection as the bias voltage increases because of weak localization, as in Ref. 21. More detailed investigations are under way to put this conjectured scenario on a microscopic basis.

The authors thank D. Feinberg and M. Houzet for helpful discussions. D. Feinberg participated in the early BTK model calculations for the NISIN structure. The authors also thank B. Douçot and J. Ranninger for introducing them to collective modes.

* U.P.R. 5001 du CNRS, Laboratoire conventionné avec l’Université Joseph Fourier

¹ A.F. Andreev, Sov. Phys. JETP **19**, 1228 (1964).

² C.J. Lambert and R. Raimondi, J. Phys.: Condens. Matter **10**, 901 (1998).

³ F.J. Jedema *et al.*, Phys. Rev. B **60**, 16549 (1999).

⁴ M.S. Choi, C. Bruder, and D. Loss, Phys. Rev. B **62**, 13569 (2000); P. Recher, E. V. Sukhorukov, and D. Loss Phys. Rev. B **63**, 165314 (2001).

⁵ G. B. Lesovik, T. Martin, and G. Blatter, Eur. Phys. J. B **24**, 287 (2001); N. M. Chtchelkatchev, G. Blatter, G. B. Lesovik, and T. Martin, Phys. Rev. B **66**, 161320(R) (2002).

⁶ J. M. Byers and M. E. Flatté, Phys. Rev. Lett. **74**, 306 (1995).

⁷ G. Deutscher and D. Feinberg, App. Phys. Lett. **76**, 487 (2000);

⁸ P. Samuelsson, E. V. Sukhorukov, and M. Büttiker, Phys. Rev. Lett. **91**, 157002 (2003).

⁹ E. Prada and F. Sols, Eur. Phys. J. B **40**, 379 (2004).

¹⁰ C. J. Lambert, J. Koltai, and J. Cserti, *Towards the Controllable Quantum States (Mesoscopic Superconductivity and Spintronics*, 119, Eds H. Takayanagi and J. Nitta, World Scientific (2003).

¹¹ R. Mélin and S. Peysson, Phys. Rev. B **68**, 174515 (2003); R. Mélin, Phys. Rev. B **72**, 134508 (2005).

¹² G. Falci, D. Feinberg, and F.W.J. Hekking, Europhysics Letters **54**, 255 (2001).

¹³ D. Feinberg, Eur. Phys. J. B **36**, 419 (2003).

¹⁴ N. M. Chtchelkatchev and I. S. Burmistrov, Phys. Rev. B **68**, 140501 (2003).

¹⁵ R. Mélin and D. Feinberg, Eur. Phys. J. B **26**, 101 (2002).

¹⁶ R. Mélin and D. Feinberg, Phys. Rev. B **70**, 174509 (2004).

¹⁷ F. Taddei and R. Fazio, Phys. Rev. B **65**, 134522 (2002).

¹⁸ G. Bignon, M. Houzet, F. Pistolesi, and F. W. J. Hekking, Europhys. Lett. **67**, 110 (2004).

¹⁹ D. Beckmann, H.B. Weber, and H. v. Löhneysen, Phys. Rev. Lett. **93**, 197003 (2004). D. Beckmann and H. v. Löhneysen, LT 24 conference proceedings, cond-mat/0512445 (2005).

²⁰ S. Russo, M. Krugl, T.M. Klapwijk, and A.F. Morpugo, Phys. Rev. Lett. **95**, 027002 (2005).

²¹ R. Mélin, cond-mat/0510837, Phys. Rev. B in press (2005).

²² P.W. Anderson, Phys. Rev. **110**, 827 (1958); Phys. Rev. **112**, 1900 (1958).

²³ N. N. Bogoliubov, J. Exptl. Theoret. Phys. U.S.S.R. **34**, 73 (1958); [Soviet Phys. JETP **34**(7), 51 (1958)].

²⁴ G.E. Blonder, M. Tinkham, and T.M. Klapwijk, Phys. Rev. B **25**, 4515 (1982).

²⁵ F.W.J. Hekking and Yu.V. Nazarov Phys. Rev. Lett. **71**,

²⁶ 1625 (1993); Phys. Rev. B **49**, 6847 (1994).
²⁶ C.W.J. Beenakker Rev. Mod. Phys. **69**, 731 (1997).
²⁷ J.A. Melsen and C.W.J. Beenakker, Physica (Amsterdam) **203B**, 219 (1994).
²⁸ T. Yamashita, S. Takahashi and S. Maekawa, Phys. Rev. B **68**, 174504 (2003); Phys. Rev. B **67**, 094515 (2003).
²⁹ E. Vecino, A. Martín-Rodero, and A. Levy Yeyati Phys. Rev. B **64**, 184502 (2001).
³⁰ A. Levy Yeyati, Phys. Rev. B **45**, 14189 (1992).
³¹ R. A. Smith and V. Ambegaokar, Phys. Rev. B **45**, 2463 (1992).
³² M. Dinter, J. Low Temp. Phys. **26**, 39 (1976).
³³ A.A. Varlamov and V.V. Dorin, Zh. Eksp. Teor. Fiz. **91**, 1955 (1986) [Sov. Phys. JETP **64**, 1159 (1986)].
³⁴ I.O. Kulik, O. Entin-Wohlman and R. Orbach, Jour. Low Temp. Phys. **43**, 591 (1981).
³⁵ L.P. Gorkov, A. Larkin, and D.E. Khmelnitskii, Pis'ma Zh. Eksp. Teor. Fiz. **30**, 248 (1979) [JETP Lett. **30**, 228 (1979)].
³⁶ S. Hikami, Phys. Rev. B **24**, 2671 (1981).
³⁷ E. Akkermans and G. Montambaux, *Physique mésoscopique des électrons et des photons*, CNRS Editions, EDP Sciences (2004).